Engineering Transactions, **71**(1): 53–79, 2023, doi: 10.24423/EngTrans.2245.20230213
Institute of Fundamental Technological Research Polish Academy of Sciences (IPPT PAN)
Université de Lorraine • Poznan University of Technology

Research Paper

Unsteady Hydromagnetic Mixed Convection of a Radiating and Reacting Nanofluid in a Microchannel with Variable Properties

Mesfin Zewde KEFENE[1)*], Oluwole Daniel MAKINDE[2)],
Lemi Guta ENYADENE[1)]

[1)] *Adama Science and Technology University, Department of Applied Mathematics*
Adama, Ethiopia; e-mail: senalemi2007@gmail.com

[2)] *Stellenbosch University, Faculty of Military Science*
Private Bag X2, Saldanha 7395, South Africa; e-mail: makinded@gmail.com

[*]Corresponding Author e-mail: mesfink2005@gmail.com

Unsteady MHD mixed convection of nanofluid heat transfer in a permeable microchannel with temperature-dependent fluid properties is studied under the influence of a first-order chemical reaction and thermal radiation. The viscosity and thermal conductivity are assumed to be related to temperature exponentially. Using suitable dimensionless variables and parameters, the governing partial differential equations (PDEs) are transformed to their corresponding dimensionless forms solved numerically by a semi-discretization finite difference scheme along with the Runge-Kutta-Fehlberg integration technique. The effects of model parameters on the profiles of velocity, temperature, concentration, skin friction, the Nusselt number, and the Sherwood number are discussed qualitatively with the aid of graph.

Keywords: nanofluid; mixed convection; permeable microchannel; Buongiorno model; thermal radiation.

1. Introduction

With technological advancement, electronic devices have shown improvements with regard to speed, dimension, and energy that they become fast in speed, miniaturized in dimension and powerful in energy. The greatest attention these days in system development is paid to the issue of enhancing the heat transfer performance of devices and optimizing the energy. Nanofluid is used in a novel technique for augmenting the heat transfer by suspending metallic or non-metallic nanoparticles with typical dimension of less than 100 nm in an ordinary fluid such as water, oil, toluene, ethylene-glycol, etc. The low thermophysical properties of these liquids have prompted using nanoparticles as an additive to improve the thermal properties and increase the heat transfer characteristics of the resulting mixture. As a result, the fluid thermal conductivity improved due to the fact that solid nanoparticles have higher thermal conductivity than the carrier liquids, and suspending them in a liquid will improve the thermal conductivity of the mixture; see Abu-Nada and Oztop [1], Choi and Eastman [6], Das *et al.* [7], Kakaç and Pramuanjaroenkij [11], Mohammed *et al.* [28], Sheikholeslami [40], Wang and Mujumdar [46], and Yu *et al.* [47].

Choi [5] is the first who coined the term nanofluid for colloidal suspensions of nanoparticles in a base fluid, in which the nanofluids show an unusual increase of effective thermal conductivity with a small nanoparticles concentration loading.

There are various devices that could use nanofluid as a working fluid; see [3, 8, 17, 19, 35, 37]. Microchannels are the ones with high heat dissipation capabilities unlike conventional heat removal devices due to their higher surface area to remove heat for a fixed volume. The first study of fluid flow and heat transfer in a microchannel was performed by Tuckerman and Pease [44]. Their result indicates that decreasing the hydraulic diameter of the microchannel will result in the enhancement of the heat transfer rate, and microchannels show a better cooling performance. However, this happens at the cost of the high pressure drop in the microchannel.

Khan and Fartaj [14] suggested that the finest design of microchannels essentially relies on the operational reliability and heat transfer performance of the channel. Utilizing nanofluid could be helpful for improving energy efficiency and heat transfer of the microchannel. As part of microfluidics and nanotechnology, nanofluid flow in microchannels has the potential for major applications in microscale cooling and nanodrug delivery, see Kleinstreuer *et al.* [16] and Li and Kleinstreuer [20].

A number of researchers have studied the problem of nanofluid flow in a microchannel [4, 12, 15, 33, 42]. Malvandi and Ganji [27] studied theoretically fully developed mixed convection of alumina/water nanofluid flow and heat transfer in a vertical microchannel in the presence of heat source/sink with asymmetric wall heat fluxes. Belhadj [2] analyzed numerically the heat transfer performance of microchannel heat sinks filled with fully developed laminar forced convection flow of water/Al_2O_3. They found that the Nusselt number increases with increasing the Reynolds number and nanoparticle concentration.

Nguyen *et al.* [32] looked at the heat transfer and entropy generation of nanofluid flow in a triangular corrugated microchannel with a wall slip velocity effect in the presence of a uniform magnetic field applied normal to the flow direction. The results affirm that the slip coefficient increased from 0 to 0.1 and improving the magnetic field enhanced the heat transfer. The combined effects of buoyancy force, magnetic field, and viscous dissipation on the steady flow of Eyring-Powell nanofluid through a vertical microchannel with convective boundary conditions was studied by Sindhu and Gireesha [41].

Studies on MHD mixed convection of a radiating and reacting nanofluid through a microchannel with variable fluid properties have considerable importance due to several applications in science and engineering. The examples include: an electrically powered micro-heat exchanger for use in the production of biodiesel fuel, the printed circuit heat exchanger (PCHE) used in petrochemical plants and fuel cells, and cell proliferation in microchannel bioreactors. It is well known that physical properties such as viscosity and thermal conductivity of the fluid depend on temperature. In many systems, the rise in temperature affects the viscosity and thermal conductivity of the fluid, so these fluid properties can no longer be assumed constant. In order to accurately predict the flow behavior, it is necessary to take in to consider the viscosity and thermal conductivity of the fluid as a function of temperature. Several authors [18, 21, 24, 36] have examined this effect in microchannel flow under various hydraulic and thermal boundary conditions. They concluded that the viscosity and thermal conductivity of a working fluid are sensitive to temperature variation. Along this line, many researchers have considered the impact of temperature-dependent fluid properties on flow and heat transfer characteristics of microchannel. Herwig and Mahulikar [9] presented variable fluid property effects in a single-phase incompressible flow through microchannels. They found that temperature dependence of fluid properties such as viscosity and thermal conductivity has a significant influence on the flows in a micro-sized pipe and channel geometry. A study of the effect of temperature-dependent thermo-physical properties on the swirl decay of an incompressible, laminar swirling flow of liquid in a heated micro-tube was carried out by Pati and Kumar [34]. It reveals that there is a significant alteration of the transport characteristics with the consideration of temperature-dependent viscosity of the fluid, while the influences of the variable density and thermal conductivity are almost insignificant. Rikitu *et al.* [38] studied unsteady mixed convection of a radiating and reacting nanofluid flow through a porous microchannel with the variable fluid property. It was found that viscosity and thermal conductivity parameters have a dwindling effect on fluid velocity and temperature distribution.

Meanwhile, various engineering flow processes occur at high temperature value in which the thermal radiation plays an important role in controlling the heat transfer in non-isothermal system, see Sparrow and Cess [43]. Thermal radiation is defined as the emission of electromagnetic waves from all matter with a temperature greater than absolute zero. Studies on the interaction between thermal radiation and nanofluid flow are very important because thermal radiation emission patterns rely on temperature and nanoparticles concentration. The dispersed nanoparticles increase the surface area of the base fluid for collecting thermal radiation and make nanofluid very useful as a solar collector, see Makinde *et al.* [25]. The interaction of radiation with mixed convection flows of variable viscosity fluid permeated by a transverse magnetic filed was studied by Makinde and Ogulu [26]. The simultaneous effects of thermal radiation, buoyancy forces, convective cooling, and viscous dissipation on inherent irreversibility and thermal stability of temperature dependent viscosity ethylene-glycol/silver (EG/Ag) nanofluid in microchannels were studied by Monaledi and Makinde [29].

Mostafazadeh *et al.* [30] investigated the flow and heat transfer characteristics of nanofluid flow in a vertical channel by considering the influence of thermal radiation with a single-phase and two-phase flow model at constant surface temperature and heat flux boundary conditions. Recently, Kefene *et al.* [13] have studied theoretically an unsteady mixed convection of MHD nanofluid flow through a permeable parallel-plates microchannel oriented vertically with temperature-dependent variable viscosity. They demonstrated the combined effects of buoyancy force, pressure gradient, thermophoresis, the Brownian motion, magnetic field, and temperature-dependent variable viscosity on mixed convection flow of conducting fluid through vertical parallel-plates microchannel with suction and injection at the walls in the absence of thermal radiation and chemical reaction.

The main objective of this study is to extend the recent work of Kefene *et al.* [13] to include the combined effects of thermal radiation, chemical reaction, and temperature-dependent thermal conductivity on transient hydromagnetic nanofluid flow in a parallel-plate permeable microchannel in the presence of convective heating boundary condition at the left wall.

2. Mathematical formulation

Consider a hydromagnetic flow of an unsteady, incompressible, chemically reacting, temperature-dependent thermal conductivity, and variable viscosity nanofluid through a vertical parallel-plates microchannel of width a units. A uniform transverse magnetic field B_0 is imposed in the direction parallel to the positive $\overline{y}$-axis, and the induced magnetic field due to the motion of a conducting nanofluid is neglected. Both fluid injection and suction are assumed to take place at the left and right walls, respectively (Fig. 1). A two-dimensional coordinate system is used where the left wall is held at $\overline{y} = 0$ and right wall is held at $\overline{y} = a$.

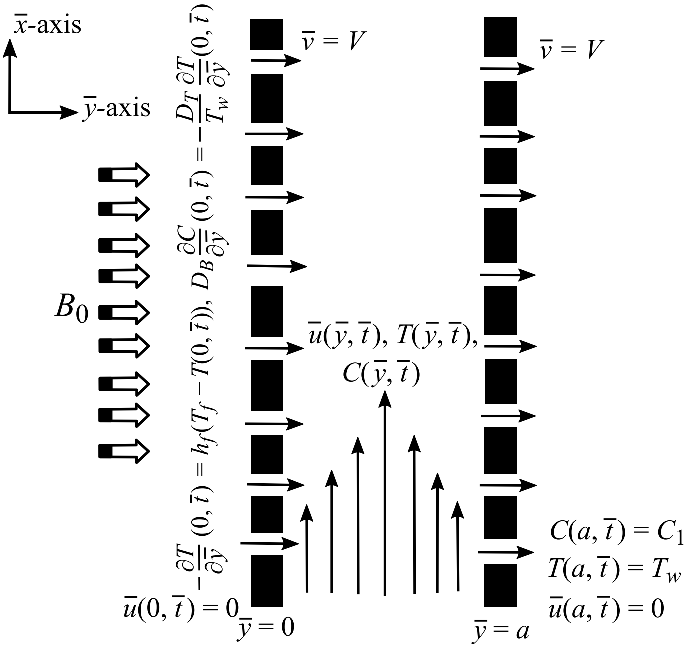

FIG. 1. Flow diagram with the coordinate system.

The nanofluid flow in the microchannel is generated due to the combined effects of pressure gradient in the $\overline{x}$-axis direction, buoyancy forces and suction/injection velocity V at the microchannel walls. The left wall $\overline{y} = 0$ of the microchannel is convectively heated by a hot fluid at a temperature T_f with coefficient of heat transfer h_f and the right wall $\overline{y} = a$ is held at a temperature of T_w, which is also equal to the fluid initial temperature. The fluid chemical compound could experience a first-order chemical reaction with the Arrhenius kinetics (in the absence of reactant consumption) and without internal heat generation in the fluid. Applying the above assumptions, the Buongiorno flow model, MHD model equations, and the usual Oberbeck-Boussinesq approximation, the basic unsteady conservation of mass, momentum, energy, and concentration equations of nanofluid flow through a microchannel in the presence of thermal radiation are written as:

$$\frac{\partial \overline{u}}{\partial \overline{x}} = 0, \tag{2.1}$$

$$\frac{\partial \overline{u}}{\partial \overline{t}} + V\frac{\partial \overline{u}}{\partial \overline{y}} = -\frac{1}{\rho}\frac{\partial \overline{P}}{\partial \overline{x}} + \frac{1}{\rho}\frac{\partial}{\partial \overline{y}}\left[\mu(T)\frac{\partial \overline{u}}{\partial \overline{y}}\right] - \frac{\sigma}{\rho}B_0^2\overline{u} + \beta_1 g(T - T_w) + \beta_2 g(C - C_0), \tag{2.2}$$

$$\frac{\partial T}{\partial \bar{t}} + V\frac{\partial T}{\partial \overline{y}} = \frac{1}{\rho c_p}\frac{\partial}{\partial \overline{y}}\left[k(T)\frac{\partial T}{\partial \overline{y}}\right] + \tau\left[D_B\frac{\partial C}{\partial \overline{y}}\frac{\partial T}{\partial \overline{y}} + \frac{D_T}{T_w}\left(\frac{\partial T}{\partial \overline{y}}\right)^2\right] + \frac{\mu(T)}{\rho c_p}\left(\frac{\partial \overline{u}}{\partial \overline{y}}\right)^2 + \frac{\sigma B_0^2}{\rho c_p}\overline{u}^2 - \frac{1}{\rho c_p}\frac{\partial q_r}{\partial \overline{y}}, \tag{2.3}$$

$$\frac{\partial C}{\partial \bar{t}} + V\frac{\partial C}{\partial \overline{y}} = D_B\frac{\partial^2 C}{\partial \overline{y}^2} + \frac{D_T}{T_w}\frac{\partial^2 T}{\partial \overline{y}^2} - \varepsilon(C - C_0), \tag{2.4}$$

with the initial and boundary conditions

$$\overline{u}(\overline{y}, 0) = 0, \qquad T(\overline{y}, 0) = T_w, \qquad C(\overline{y}, 0) = C_0, \tag{2.5}$$

$$\begin{aligned} &\overline{u}(0, \bar{t}) = 0, && \overline{u}(a, \bar{t}) = 0,\\ &-k_0\frac{\partial T}{\partial \overline{y}}(0, \bar{t}) = h_f[T_f - T(0, \bar{t})], && T(a, \bar{t}) = T_w,\\ &D_B\frac{\partial C}{\partial \overline{y}}(0, \bar{t}) = -\frac{D_T}{T_w}\frac{\partial T}{\partial \overline{y}}(0, \bar{t}), && C(a, \bar{t}) = C_1. \end{aligned} \tag{2.6}$$

The expressions for dynamic viscosity $\mu(T)$ and thermal conductivity $k(T)$ of nanofluid are:

$$\mu(T) = \mu_0 e^{-\gamma_1(T - T_w)}, \tag{2.7}$$

$$k(T) = k_0 e^{\gamma_2(T - T_w)}, \tag{2.8}$$

where $\overline{u}$ is the nanofluid velocity in the $\overline{x}$-direction, T is the temperature of nanofluid, C is the nanoparticle concentration, V is the suction/injection velocity, $\overline{P}$ is the nanofluid pressure, $\bar{t}$ is time, ρ is the density of nanofluid, μ is the dynamic viscosity of the nanofluid, g is the acceleration due to gravity, β_1 and β_2 are the thermal and solutal expansion coefficients, respectively, k is the thermal conductivity of the nanofluid, τ is the ratio between the effective heat capacity of nanoparticle material and heat capacity of the base fluid, D_T is the thermophoretic diffusion coefficient, D_B is the Brownian motion diffusion coefficient, q_r is the thermal radiative heat flux, ε the reaction rate, T_w is nanofluid initial temperature (nanofluid temperature at the right wall), C_0 is the nanofluid initial concentration, C_1 is the nanofluid concentration at the right wall, σ is the nanofluid electrical conductivity, a is the channel width, c_p is the specific heat at constant pressure, μ_0 is the nanofluid viscosity at temperature T_w and concentration C_0, k_0 is the nanofluid thermal conductivity at temperature T_w and concentration C_0, γ_1 is the viscosity variation coefficient, and γ_2 is the thermal conductivity variation coefficient.

The radiative heat flux, using Rosseland's approximation [39], can be written as:

$$q_r = -\frac{4\sigma^*}{3k^*}\frac{\partial T^4}{\partial \overline{y}}, \tag{2.9}$$

in which σ^* is the Stefan-Boltzman constant and k^* is the mean absorption coefficient. Assuming the difference of the temperature T of flowing fluid and hot fluid temperature T_f heating the left wall is small so that the temperature T^4 can be linearized as:

$$T^4 \approx 4T_f^3 T - 3T_f^4, \tag{2.10}$$

using Taylor's series expansion and ignoring second and higher-order terms in the expansion.

Substituting Eq. (2.10) into Eq. (2.9), we obtain

$$\frac{\partial q_r}{\partial \overline{y}} = -\frac{16\sigma^* T_f^3}{3k^*}\frac{\partial^2 T}{\partial \overline{y}^2}. \tag{2.11}$$

To transform Eqs. (2.2)–(2.6) into non-dimensional form, we introduce the following dimensionless variables and parameters:

$$\begin{aligned}
&x = \frac{\overline{x}}{a}, && y = \frac{\overline{y}}{a}, && u = \frac{\overline{u}a}{\nu_0},\\
&t = \frac{\nu_0 \overline{t}}{a^2}, && \theta = \frac{T - T_w}{T_f - T_w}, && \phi = \frac{C - C_0}{C_1 - C_0},\\
&\overline{P} = \frac{\nu_0^2 P}{\rho a^2}, && \mathrm{Re} = \frac{Va}{\nu_0}, && A = -\frac{\mathrm{d}p}{\mathrm{d}x},\\
&A_1 = \gamma_1(T_f - T_w), && M^2 = \frac{\sigma B_0^2 a^2}{\rho \nu_0}, && \mathrm{Gr} = \frac{\beta_1 g a^3 (T_f - T_w)}{\nu_0^2},\\
&\mathrm{Gc} = \frac{\beta_2 g a^3 (C_1 - C_0)}{\nu_0^2}, && \mathrm{Pr} = \frac{\nu_0}{\alpha_0}, && \mathrm{Nb} = \frac{\tau D_B (C_1 - C_0)}{\nu_0},\\
&\mathrm{Nt} = \frac{\tau D_T (T_f - T_w)}{T_0 \nu_0}, && A_2 = \gamma_2(T_f - T_w), && \mathrm{Ec} = \frac{\nu_0^2}{a^2 c_p (T_f - T_w)},\\
&\mathrm{Nr} = \frac{4\sigma^* T_f^3}{k^* k_0}, && \mathrm{Sc} = \frac{\nu_0}{D_B}, && \mathrm{rx} = \frac{\varepsilon a^2}{\nu_0},\\
& && \mathrm{Bi} = \frac{a h_f}{k_0}. &&
\end{aligned} \tag{2.12}$$

Substituting Eqs. (2.11) and (2.12) into Eqs. (2.1)–(2.6), we obtain a system of dimensionless PDEs:

$$\frac{\partial u}{\partial t} + \mathrm{Re}\frac{\partial u}{\partial y} = A - A_1 \cdot e^{-A_1\theta}\frac{\partial \theta}{\partial y}\frac{\partial u}{\partial y} + e^{-A_1\theta}\frac{\partial^2 u}{\partial y^2} - M^2 u + \mathrm{Gr}\cdot\theta + \mathrm{Gc}\cdot\phi, \tag{2.13}$$

$$\begin{aligned}\mathrm{Pr}\frac{\partial \theta}{\partial t} + \mathrm{Pr}\cdot\mathrm{Re}\frac{\partial \theta}{\partial y} = {} & A_2 \cdot e^{A_2\theta}\left(\frac{\partial \theta}{\partial y}\right)^2 + \mathrm{Pr}\cdot\mathrm{Nb}\frac{\partial \phi}{\partial y}\frac{\partial \theta}{\partial y} \\ & + \mathrm{Pr}\cdot\mathrm{Nt}\left(\frac{\partial \theta}{\partial y}\right)^2 + \mathrm{Pr}\cdot\mathrm{Ec}\left(\frac{\partial u}{\partial y}\right)^2 e^{-A_1\theta} \\ & + \mathrm{Pr}\cdot M^2\cdot\mathrm{Ec}\cdot u^2 + \left(e^{A_2\theta} + \frac{3}{4}\mathrm{Nr}\right)\cdot\frac{\partial^2 \theta}{\partial y^2},\end{aligned} \tag{2.14}$$

$$\mathrm{Nb}\cdot Sc\frac{\partial \phi}{\partial t} + \mathrm{Nb}\cdot\mathrm{Re}\cdot\mathrm{Sc}\frac{\partial \phi}{\partial y} = \mathrm{Nb}\cdot\frac{\partial^2 \phi}{\partial y^2} + \mathrm{Nt}\cdot\frac{\partial^2 \theta}{\partial y^2} - \mathrm{Nb}\cdot\mathrm{Sc}\cdot\mathrm{rx}\cdot\phi, \tag{2.15}$$

with initial and boundary conditions

$$u(y,0) = 0, \qquad \theta(y,0) = 0, \qquad \phi(y,0) = 0, \tag{2.16}$$

$$\begin{aligned} & u(0,t) = 0, && u(1,t) = 0, \\ & \frac{\partial \theta}{\partial y}(0,t) = \mathrm{Bi}[\theta(0,t) - 1], && \theta(1,t) = 0, \\ & \mathrm{Nb}\frac{\partial \phi}{\partial y}(0,t) = -\mathrm{Nt}\frac{\partial \theta}{\partial y}(0,t), && \phi(1,t) = 1, \end{aligned} \tag{2.17}$$

where Re is the Reynolds suction/injection parameter, A is the pressure gradient parameter, A_1 is the variable viscosity variation parameter, M is the magnetic field parameter, Gr is the thermal Grashof number, Gc is the solutal/mass Grashof number, Pr is the Prandtl number, Nb is the Brownian motion parameter, Nt is the thermophoretic parameter, A_2 is the variable thermal conductivity variation parameter, Ec is the Eckert number, Nr is thermal radiation parameter, Sc is the Schmidt number, rx is chemical reaction parameter, and Bi is the Biot number.

The quantities of practical interest in the study of the problem are the skin friction Cf, the Nusselt number Nu, and the Sherwood number Sh which are defined as

$$\mathrm{Cf} = \frac{\tau_w}{\rho V^2}, \qquad \mathrm{Nu} = \frac{a q_w}{k(T)[T_f - T_w]}, \qquad \mathrm{Sh} = \frac{a q_m}{D_B(C_1 - C_0)}, \tag{2.18}$$

where τ_w is the wall shear stress, q_w is the heat flux, and q_m is the mass flux at the left and right walls of the microchannel and are given by

$$\tau_w = \mu \left.\frac{\partial \overline{u}}{\partial \overline{y}}\right|_{\overline{y}=0,a}, \qquad q_w = -k \left.\frac{\partial T}{\partial \overline{y}}\right|_{\overline{y}=0,a}, \qquad q_m = -D_B \left.\frac{\partial C}{\partial \overline{y}}\right|_{\overline{y}=0,a}. \tag{2.19}$$

The dimensionless form of Eq. (2.18) above are:

$$\begin{gathered}\mathrm{Re}^2\mathrm{Cf} = e^{-A_1\theta} \left.\frac{\partial u}{\partial y}\right|_{y=0,1}, \qquad \mathrm{Nu} = -\left(1 + \frac{4}{3}e^{-A_1\theta}\mathrm{Nr}\right) \cdot \left.\frac{\partial \theta}{\partial y}\right|_{y=0,1}, \\ \mathrm{Sh} = -\left.\frac{\partial \phi}{\partial y}\right|_{y=0,1}.\end{gathered} \tag{2.20}$$

3. Numerical method

The model nonlinear Eqs. (2.13)–(2.17) are a system of initial boundary value problems (IBVPs) and their solutions are obtained by using a semi-discretization via a finite difference scheme with the Runge-Kutta-Fehlberg integration technique. A spatial interval [0, 1] is subdivided into $N + 1$ equal subintervals. The nodal spacing and points are defined, respectively, as $\Delta y = \frac{1}{N+1}$ and $y_i = i\Delta y$, for $i = 0, 1, 2, ..., N + 1$. The first and second spatial derivatives are replaced by a finite difference approximation of order $(\Delta y)^2$ accuracy. Let u_i, θ_i, and ϕ_i represent $u(y_i, t)$, $\theta(y_i, t)$, and $\phi(y_i, t)$, respectively. Then the semi-discretization scheme with centered finite difference method for Eqs. (2.13)–(2.17) reduces to:

$$\begin{aligned}\frac{\mathrm{d}u_i}{\mathrm{d}t} + \mathrm{Re}\left(\frac{u_{i+1} - u_{i-1}}{2\Delta y}\right) &= A - A_1 e^{-A_1\theta_i}\left(\frac{\theta_{i+1} - \theta_{i-1}}{2\Delta y}\right)\left(\frac{u_{i+1} - u_{i-1}}{2\Delta y}\right) \\ &+ e^{-A_1\theta_i}\left(\frac{u_{i+1} - 2u_i + u_{i-1}}{(\Delta y)^2}\right) - M^2 u_i + \mathrm{Gr}\,\theta_i + \mathrm{Gc}\,\phi_i,\end{aligned} \tag{3.1}$$

$$\begin{aligned}\mathrm{Pr}\frac{\mathrm{d}\theta_i}{\mathrm{d}t} + \mathrm{Pr}\;\mathrm{Re}\left(\frac{\theta_{i+1} - \theta_{i-1}}{2\Delta y}\right) &= A_2 e^{A_2\theta_i}\left(\frac{\theta_{i+1} - \theta_{i-1}}{2\Delta y}\right)^2 \\ &+ \mathrm{Pr}\;\mathrm{Nb}\left(\frac{\phi_{i+1} - \phi_{i-1}}{2\Delta y}\right)\left(\frac{\theta_{i+1} - \theta_{i-1}}{2\Delta y}\right) \\ &+ \mathrm{Pr}\;\mathrm{Nt}\left(\frac{\theta_{i+1} - \theta_{i-1}}{2\Delta y}\right)^2 + \mathrm{Pr}\;\mathrm{Ec} \cdot e^{-A_1\theta_i}\left(\frac{u_{i+1} - u_{i-1}}{2\Delta y}\right)^2 \\ &+ \mathrm{Pr}\,M^2\mathrm{Ec} \cdot u_i^2 + \left(e^{A_2\theta_i} + \frac{4}{3}\mathrm{Nr}\right)\left(\frac{\theta_{i+1} - 2\theta_i + \theta_{i-1}}{(\Delta y)^2}\right),\end{aligned} \tag{3.2}$$

$$\text{Sc}\frac{\text{d}\phi_i}{\text{d}t} + \text{Re Sc Nb}\left(\frac{\phi_{i+1}-\phi_{i-1}}{2\Delta y}\right) = \text{Nb}\left(\frac{\phi_{i+1}-2\phi_i+\phi_{i-1}}{(\Delta y)^2}\right) + \text{Nt}\left(\frac{\theta_{i+1}-2\theta_i+\theta_{i-1}}{(\Delta y)^2}\right) - \text{rx}\cdot\phi_i, \tag{3.3}$$

with initial conditions

$$u_i(0) = 0, \qquad \theta_i(0) = 0, \qquad \phi_i(0) = 0, \qquad 1 \le i \le N. \tag{3.4}$$

The boundary conditions at $y = 0, 1$ are transformed to incorporate as follows:

$$\begin{aligned} &u_0(t) = 0, && u_{N+1}(t) = 0,\\ &\theta_1(t) = \theta_0(t)[1 + \text{Bi}\,\Delta y] - \text{Bi}\,\Delta y, && \theta_{N+1}(t) = 1,\\ &\phi_1(t) = \phi_0(t) - \frac{\text{Nt}}{\text{Nb}}[\theta_1(t) - \theta_0(t)], && \phi_{N+1}(t) = 1. \end{aligned} \tag{3.5}$$

Equations (3.1)–(3.5) form a system of first-order nonlinear ordinary differential equations with known initial conditions and its solution can be obtained successively by Runge-Kutta-Fehlberg integration technique, see Na [31].

4. Results and discussion

The combined effect of the magnetic field, temperature-dependent variable viscosity and thermal conductivity, first-order chemical reaction, and thermal radiation on unsteady nanofluid flow through a vertical microchannel with permeable walls was studied. Numerical solutions to nonlinear initial boundary value problems were carried out by semi-discretization via the centered finite difference method with the Runge-Kutta-Fehlberg integration technique. Results of representative velocity field, temperature field, nanoparticle concentration, skin friction, the Nusselt number and the Sherwood number were analyzed by using thermophysical parameter values $\text{Re} = M = \text{Gc} = \text{Gr} = \text{Nt} = \text{Ec} = A_1 = A_2 = \text{rx} = 0.1$, $\text{Nb} = \text{Nr} = \text{Bi} = 0.5$, $\text{Sc} = 0.6$, $\text{Pr} = 6.2$, $A = 1$, unless it is stated otherwise in Figs. 2–23.

4.1. Time evolution of velocity, temperature, and concentration profiles

The time evolution of flow velocity, temperature, and concentration profiles are highlighted in Figs. 2–5 for fixed values of thermophysical parameters. Figure 2a indicates that nanofluid velocity of zero value in space and time at both microchannel walls $y = 0$ and $y = 1$ starts growing to attain its maximum value around the hub of the channel width. Decreasing of nanofluid temperature from its ceiling value near the left wall to its zero value at/around the right

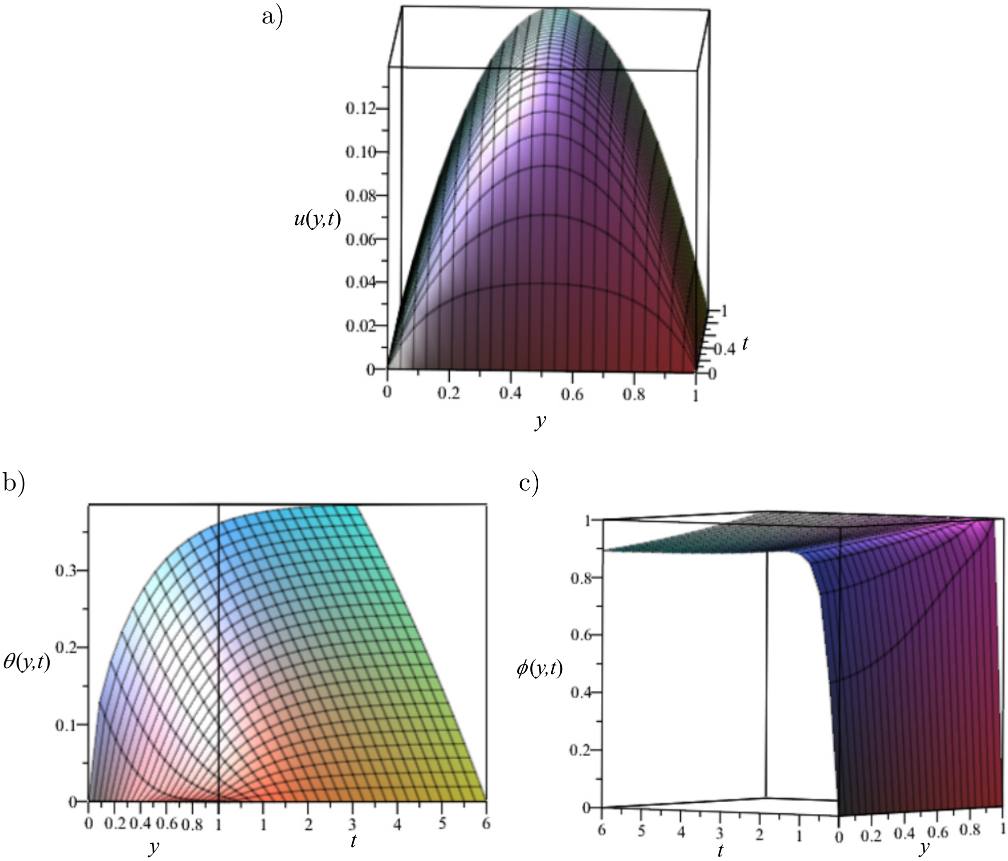

FIG. 2. Three-dimensional velocity, temperature, and concentration profile: a) 3D velocity profile, b) 3D temperature profile, c) 3D concentration profile.

wall of the microchannel is observed, but there is an increase in temperature for a fixed point in the channel width as time increases for a certain while, as depicted in Fig. 2b. The rise of nanoparticle concentration from its minimum value in space and time at the left wall to its highest value of 1 at the right wall of the microchannel is observed in Fig. 2c. In Fig. 3, as time increases, the nanofluid flow velocity attains its maximum value at the center of the microchannel before a steady-state velocity value is reached.

Moreover, the steady-state flow velocity obtained nearly $t = 2$ units. It is noted in Fig. 4a that the nanofluid temperature is maximum at the left wall and decreases toward the right wall of the microchannel until a steady-state profile is attained for a given set of parameter values. The nanofluid temperature along the microchannel flow direction increases with increasing time and reaches its minimum value at the right wall of the microchannel, as demonstrated in Fig. 4b. It can be noticed in Fig. 5 that nanoparticle concentration in the fluid increases

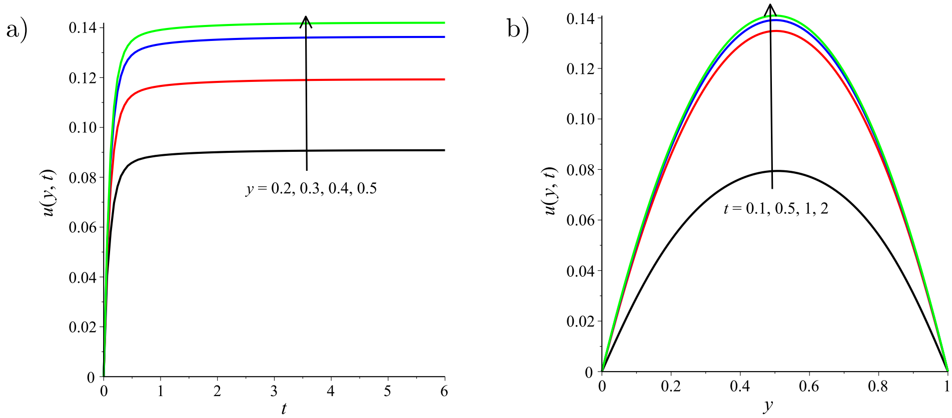

FIG. 3. Velocity profile across the channel: a) with increasing y, b) with increasing time t.

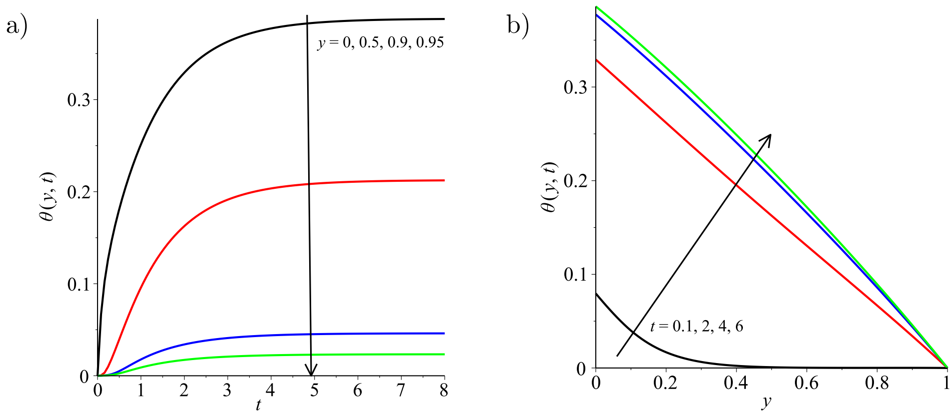

FIG. 4. Temperature profile across the channel: a) with increasing y, b) with increasing time t.

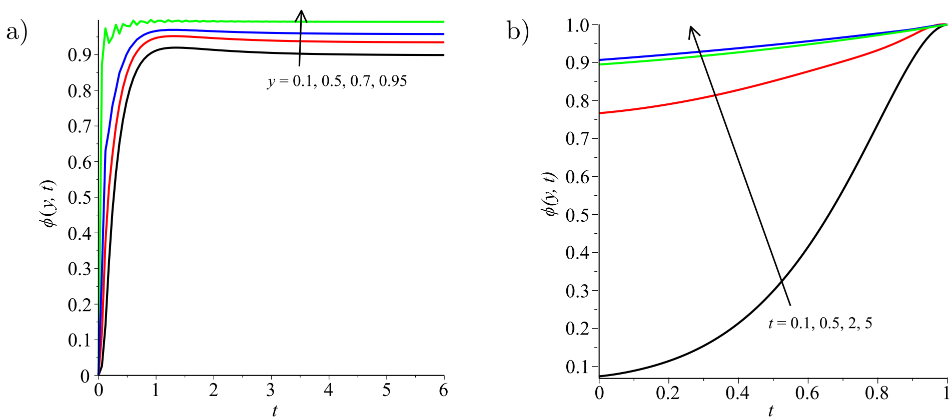

FIG. 5. Concentration profile across the channel: a) with increasing y, b) with increasing time t.

across the whole microchannel width until a steady-state constant concentration value is achieved. But, there is a dynamic fluctuation of particle concentration in the fluid near the right wall $y = 1$ of the microchannel for $0 < t < 2$.

4.2. Effects of model parameters on steady-state velocity profiles

Figures 6–8 display the steady-state velocity profiles for various values of model parameter variation. It is worth noting that the maximum nanofluid velocity is attained around the center line of the microchannel while its minimum value is at both permeable walls. The effect of suction/injection parameter Re on nanofluid velocity is illustrated in Fig. 6. It is seen in Fig. 6a that the nanofluid velocity decreases around the left wall, followed by a wavering of fluid velocity around the centerline, and it increases near the right permeable wall with an increase in suction parameter Re > 0. In Fig. 6b, as injection parameter Re > 0 increases, the velocity of the fluid increases around the left wall, followed by a fluctuation of velocity for a short while before a decrease of velocity happens. The impacts of thermal and solutal Grashof numbers Gr, Gc on the nanofluid velocity are presented in Fig. 7a. The nanofluid velocity overshoot with an increase in both Grashof numbers. This is due to increased buoyancy force, which favors the fluid flow. This outcome agrees exactly with the result of Hindebu *et al.* [10]. Figure 7b presents the effects of the viscosity variation parameter A_1 on the nanofluid velocity in the presence and absence of pressure gradient A. Increment of A_1 tends to increase the nanofluid velocity in the presence and absence of A. This is in line with the observation made by Monaledi and Makinde [29], Kefene *et al.* [13], and Makinde [22]. But a significant overshoot of velocity is observed in the presence of A. Figure 8a presents nanofluid velocity variation with chemical reaction parameter rx and magnetic field M. It is found that there is a considerable decline of nanofluid velocity as

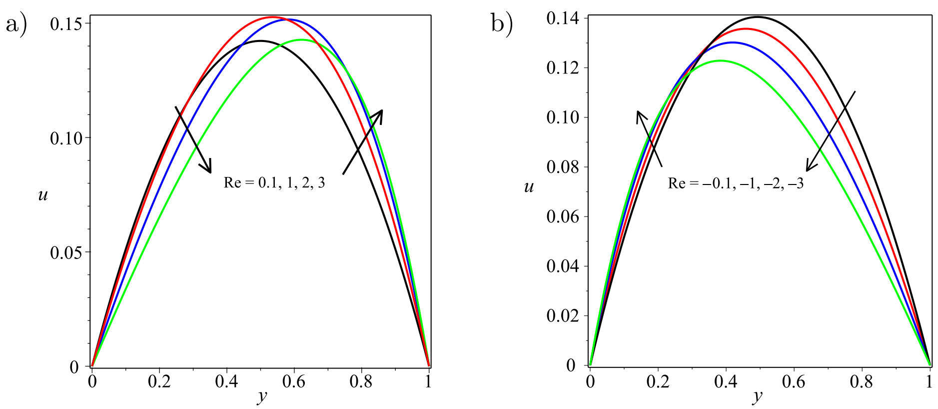

Fig. 6. Steady-state velocity profiles with increasing Re: a) Re > 0, b) Re < 0.

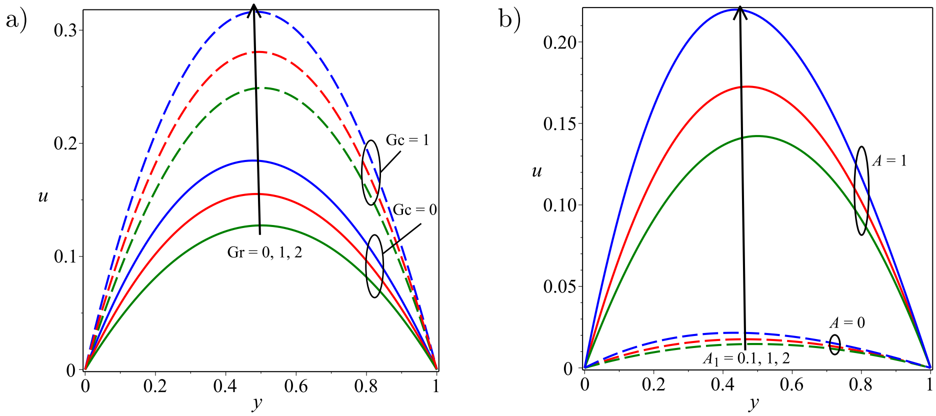

FIG. 7. Steady-state velocity profiles with increasing Gr, Gc (a) and A_1, A (b).

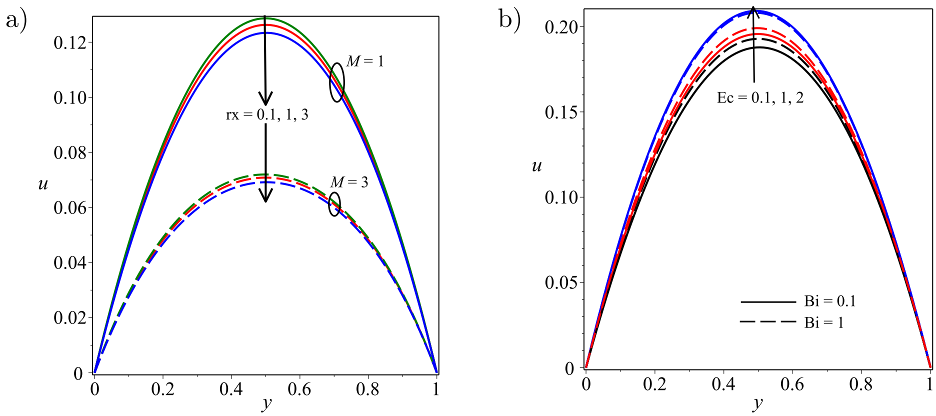

FIG. 8. Steady-state velocity profiles with increasing rx, M (a) and Ec, Bi (b).

magnetic field M and chemical reaction parameter rx increase simultaneously. The magnetic field is found to reduce the velocity across the microchannel. This is because the magnetic field provides a resisting type of force called the Lorentz force. This force tends to lessen the motion of the fluid, and as a result, the velocity reduces. The rise of the Eckert number Ec and the Biot number Bi shows an increment in the nanofluid velocity, as depicted in Fig. 8b. Here, MAKINDE and EEGUNJOBI [23] presented a similar result. However, the Biot number has no significant impact on nanofluid velocity for large values of Eckert numbers.

4.3. Effects of model parameters on steady-state temperature profiles

The variation of nanofluid temperature is illustrated in Fig. 9a with suction/injection parameters Re, in Fig. 9b with the viscosity variation parameter

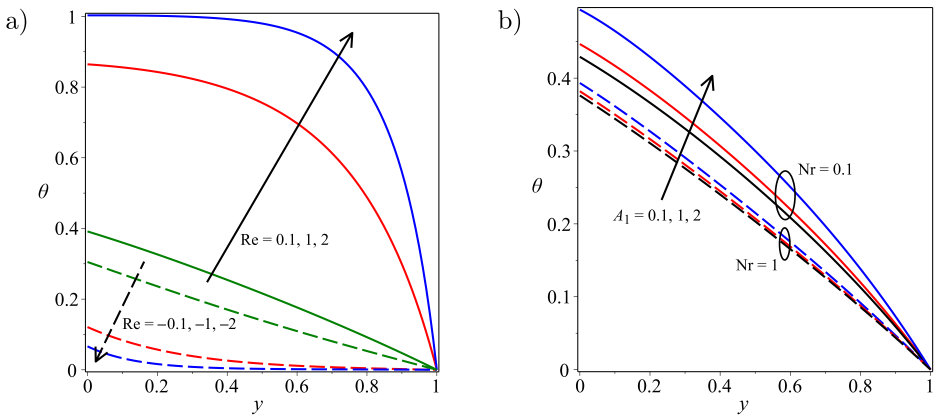

FIG. 9. Steady-state temperature profiles with increasing Re (a) and A_1, Nr (b).

A_1 and the thermal radiation parameter Nr, in Fig. 10a with the thermal conduction variation parameter A_2 and the Biot number Bi, and in Fig. 10b with the Eckert number Ec and the chemical reaction parameter rx.

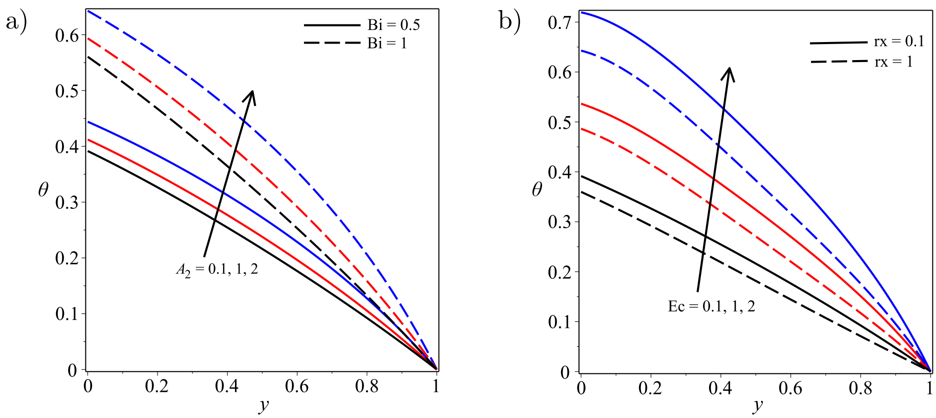

FIG. 10. Steady-state temperature profiles with increasing A_2, Bi (a) and Ec, rx (b).

In general, the nanofluid temperature is maximum at the left wall and it continues to decrease across the channel width to attain a minimal value at the right wall. An increase suction parameter Re > 0 tends to increase the nanofluid temperature, whereas the injection parameter Re < 0 helps to decrease the nanofluid temperature in the microchannel. A more significant influence of the suction/injection parameter Re on the nanofluid temperature is found across the microchannel width except near the right wall of the microchannel. Figure 9b demonstrates the influence of the viscosity variation parameter A_1 and the thermal radiation parameter Nr. It is evident that the nanofluid temperature rises as A_1 increases whereas an opposite effect is seen when Nr increases. In this instance, the results are similar to the previous outcomes reported by Monaledi and Makinde [29]. The thermal conductivity variation parameter A_2 and the Biot number Bi tend to increase the nanofluid temperature observed in Fig. 10b. As the thermal conductivity parameter A_2 increases, the heat is more readily transferred, particularly in nanofluid, which leads to the enhancement of nanofluid temperature in the microchannel. In Fig. 10b, the Eckert number Ec helps to increase the nanofluid temperature, while the chemical reaction parameter rx tend to decrease it.

4.4. Effects of model parameters on steady-state concentration profiles

The nanoparticle concentration profiles under the influence of the Schmidt number and the Brownian motion parameter (Sc, Nb), the Biot number and radiation parameter (Bi, Nr), the chemical reaction parameter (generating/degenerating) (rx $<$ 0, rx $>$ 0), and the Eckert number and the chemical reaction parameter (Ec, rx) are shown in Figs. 11 and 12, respectively. The nanoparticle concentration in the nanofluid flow field through microchannel decreased with a rise in the Schmidt number Sc, the Brownian motion parameter Nb, the Biot number Bi, and the thermal radiation parameter Nr and this is illustrated in Fig. 11.

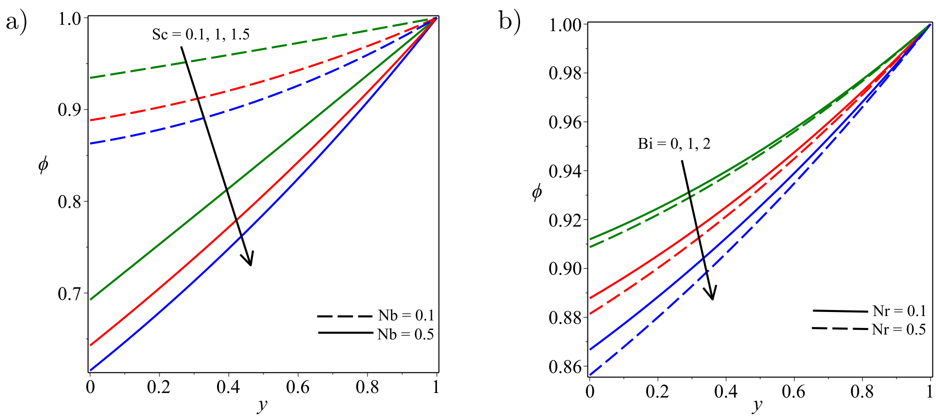

Fig. 11. Steady-state concentration profiles with increasing Sc, Nb (a) and Bi, Nr (b).

With respect to the chemical reaction parameter rx, the nanoparticle concentration enhanced with an increase in generating chemical reaction parameter rx $<$ 0, whereas the nanoparticle concentration reduce in degenerating chemical reaction parameter rx $>$ 0 in the nanofluid flow field throughout the microchannel as depicted in Fig. 12a. This result is in agreement with the preceding observation by Ullah *et al.* [45]. Physically, degenerative chemical reaction leads

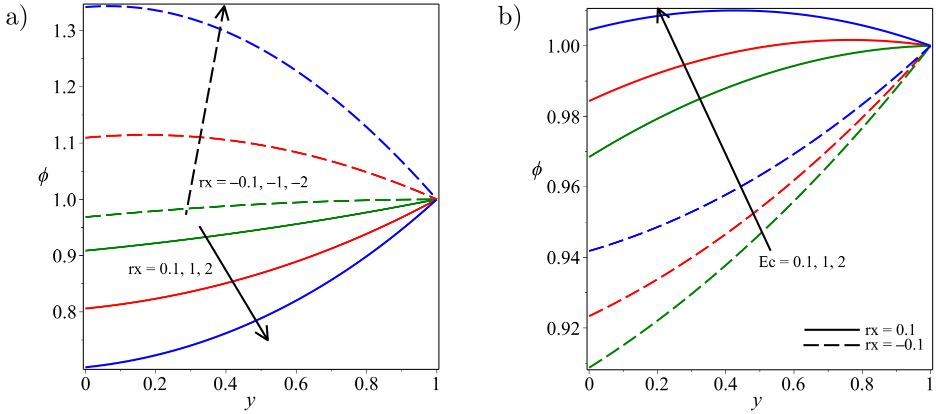

FIG. 12. Steady-state concentration profiles with increasing rx (rx < 0, rx > 0) (a) and Ec, rx (b).

to enhancing the decomposition rate of reactant species, whereas generative chemical reaction helps diffusing nanoparticles. The nanoparticle concentration profile for different values of the Eckert number Ec in the presence of degenerating/generating chemical reaction parameter rx is shown in Fig. 12b. It is observed that an enhancement of nanoparticle concentration in the flow field across the microchannel in the presence of both degenerating/generating chemical reaction parameter rx occurs.

4.5. Skin friction, Nusselt number, and Sherwood number

The effects of various thermophysical parameters on the skin friction, the Nusselt number, and the Sherwood number are shown in Figs. 13–22. It is ob-

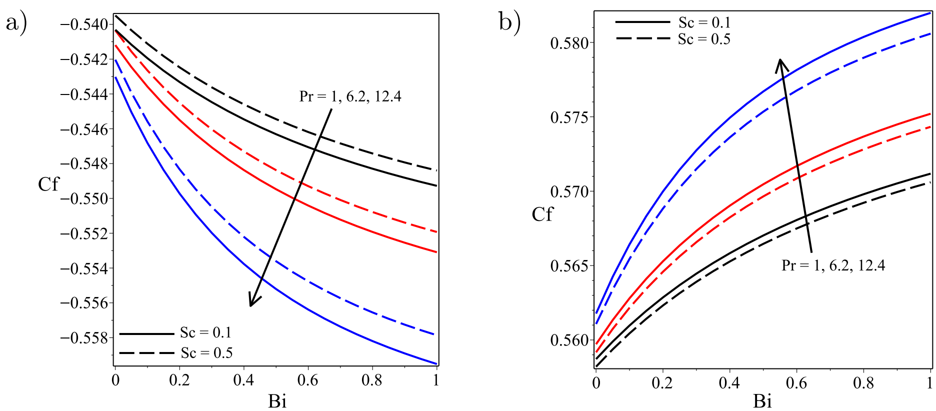

FIG. 13. Skin friction Cf vs. Biot number Bi with increasing Pr and Sc: a) at $y = 0$, b) at $y = 1$.

served in Fig. 13 that increasing Bi and Pr dwindles the skin friction Cf at the left wall $y = 0$ and increases skin friction at the right wall $y = 1$. Meanwhile, a rise in Sc increases the skin friction at the left wall $y = 0$ and decreases it at the right wall $y = 1$. In Fig. 14, increasing both the thermal Grashof number Gr and the solutal Grashof number Gc diminishes the skin friction Cf at the wall $y = 0$ and intensifies Cf at the wall $y = 1$. However, the thermal radiation parameter Nr augments Cf at $y = 0$ and reduces it at $y = 1$. The combined rise of the chemical reaction parameter $\mathrm{rx} > 0$ and the magnetic field parameter M increases the skin friction Cf at the wall $y = 0$ and decreases the skin friction Cf at the wall $y = 1$ in the existence of both suction and injection, as illustrated in Fig. 15.

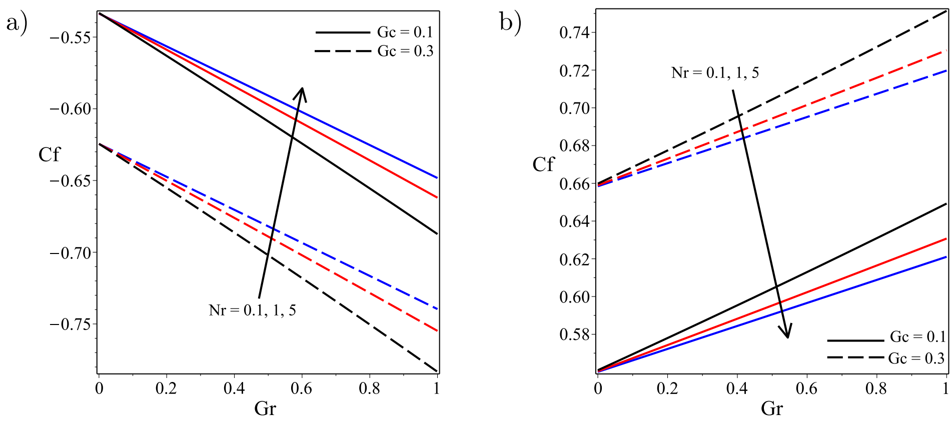

FIG. 14. Skin friction Cf vs. Grashof number Gr with increasing Nr and Gc: a) at $y = 0$, b) at $y = 1$.

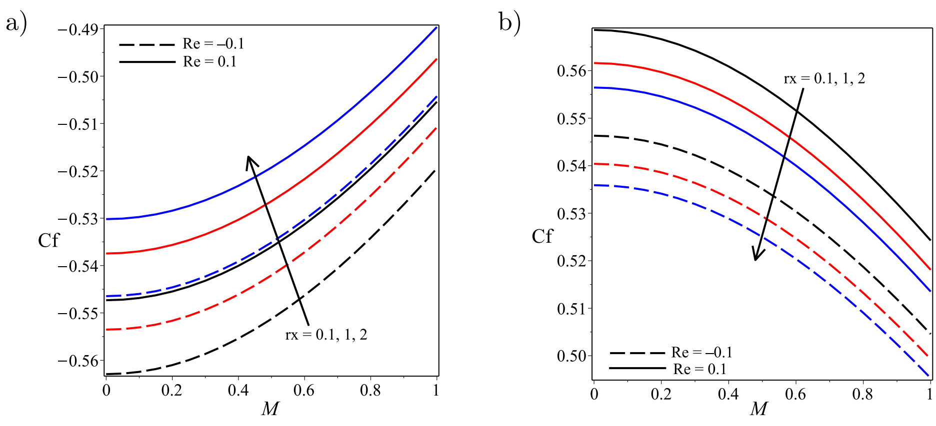

FIG. 15. Skin friction Cf vs. magnetic field parameter M with increasing rx and Re: a) at $y = 0$, b) at $y = 1$.

The effects of various model parameters on the Nusselt number at both microchannel walls ($y = 0$, $y = 1$) are illustrated in Figs. 16–18. Figure 16 presents the combined effects of the pressure gradient A, the thermal conductivity variation parameter A_2, and the Brownian motion parameter Nb on the Nusselt number at the walls $y = 0$ and $y = 1$, respectively. In these figures, it is clear that the Nusselt number increases with an increase in Nb and decreases with an increase in A at the wall $y = 0$, while a reverse trend is observed at the wall $y = 1$ with an increase in Nb and A. It is also observed that the thermal conductivity variation parameter A_2 has an increasing effect on the Nusselt number at both left $y = 0$ and right $y = 1$ walls of the microchannel. This is because the working fluid become hotter, which leads to the fluid temperature gradient augmentation at both walls since the thermal conductivity is dependent on temperature. In Fig. 17, an increase in the Eckert number Ec and the magnetic field

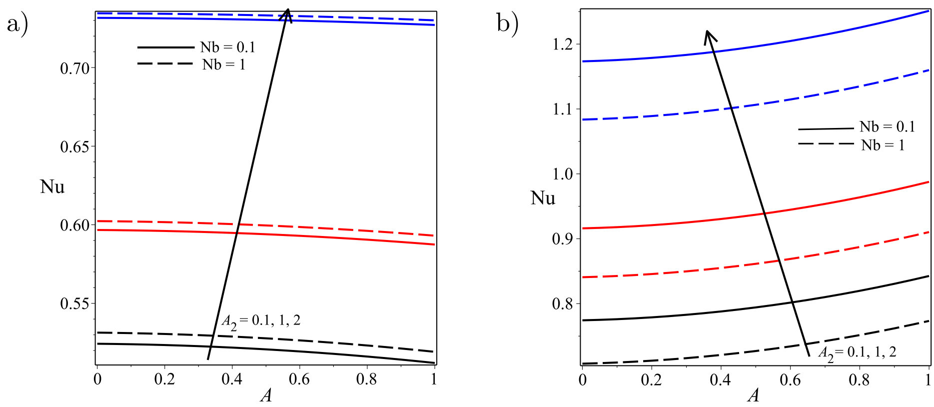

FIG. 16. Nusselt number Nu vs. pressure gradient A with increasing A_2 and Nb: a) at $y = 0$, b) at $y = 1$.

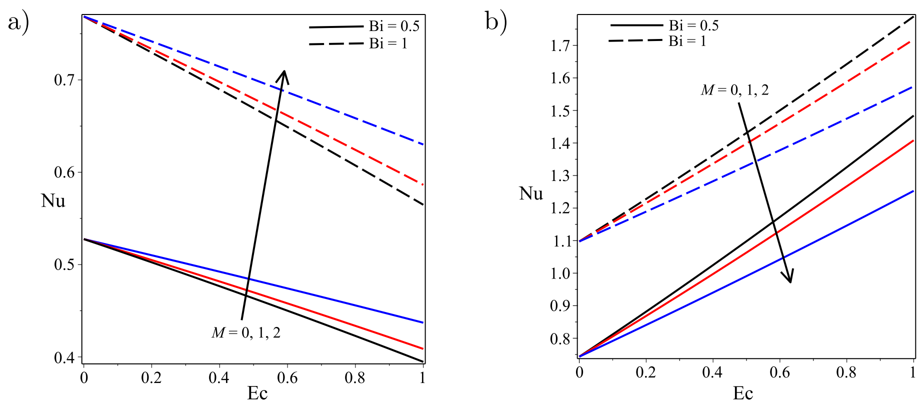

FIG. 17. Nusselt number Nu vs. Eckert number Ec with increasing M and Bi: a) at $y = 0$, b) at $y = 1$.

parameter M, respectively, helps to decrease and increase the Nusselt number at the left wall $y = 0$ whereas an opposite phenomenon happened at the right wall $y = 1$ of the microchannel. In addition, the Nusselt number Nu increases with increasing the Biot number Bi at both left $y = 0$ and right $y = 1$ walls of the microchannel. This is due to the fact that the higher the Biot number Bi means higher level of convective heating (temperature gradient) at the left wall $y = 0$ (as it can be seen in temperature boundary condition Eq. (2.17)) and hence the overall temperature profile increases with increasing the Biot number Bi. This attributes to a rise in the heat transfer rate at both walls $y = 0$ and $y = 1$ of the microchannel, which results in an increase in the Nusselt number Nu at both walls $y = 0$ and $y = 1$ of the microchannel. The change of the Nusselt number Nu vs. the Schmidt number Sc for various values chemical reaction parameter $\mathrm{rx} > 0$ with the Eckert number $\mathrm{Ec} = -0.1$ (heating) and $\mathrm{Ec} = 0.1$ (cooling) at the walls $y = 0$ and $y = 1$ is portrayed in Fig. 18. It is observed that Sc and $\mathrm{rx} > 0$ help to augment the Nusselt number Nu at both walls $y = 0$ and $y = 1$ of the microchannel with joint existence of $\mathrm{Ec} = -0.1$ (heating) and $\mathrm{Ec} = 0.1$ (cooling).

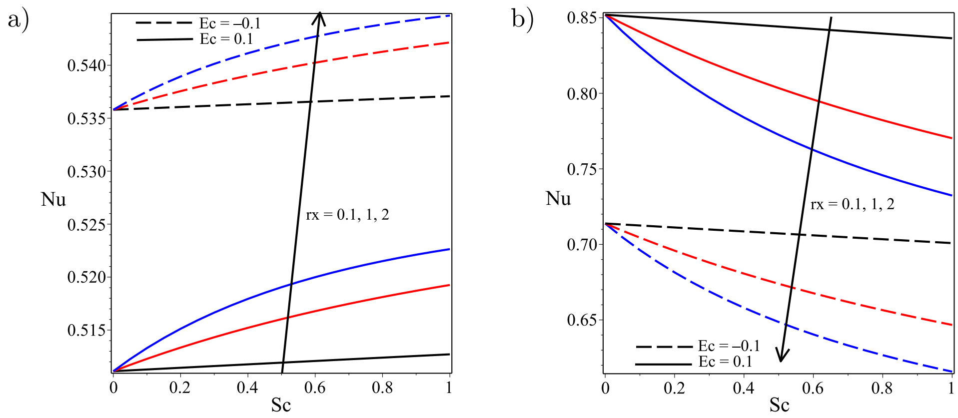

FIG. 18. Nusselt number Nu vs. Schmidt number Sc with increasing rx and Ec: a) at $y = 0$, b) at $y = 1$.

Moreover, Fig. 19 reveals the variation of the Nusselt number Nu against the Prandtl number Pr with changing values of thermal radiation parameter Nr in the presence of both suction ($\mathrm{Re} > 0$) and injection ($\mathrm{Re} < 0$) at the walls $y = 0$ and $y = 1$. Enhancement of the thermal radiation parameter Nr proliferates the Nusselt number Nu at both channel walls ($y = 0$ and $y = 1$) for the case of suction and injection. Further, a slight increment when $\mathrm{Re} < 0$ and decrement when $\mathrm{Re} > 0$ of the Nusselt number Nu is seen at the wall $y = 0$ with a rise in the Prandtl number Pr. Nevertheless, a significant opposite trend of Nu is observed at the wall $y = 1$.

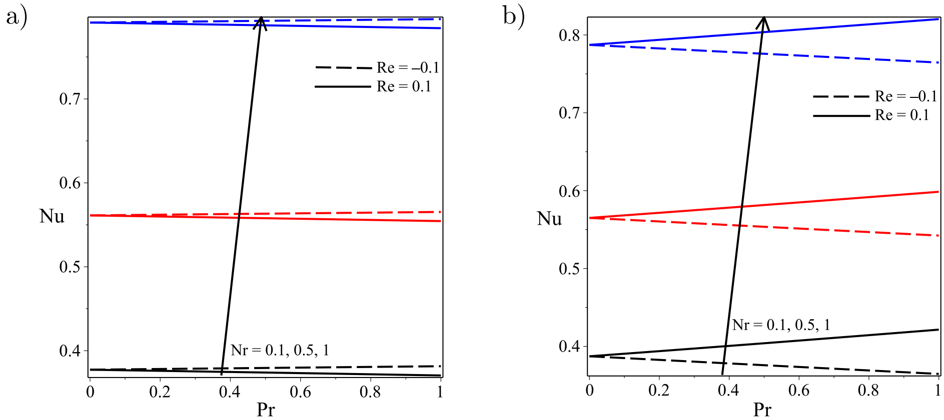

FIG. 19. Nusselt number Nu vs. Prandtl number Pr with increasing Nr and Re: a) at $y = 0$, b) at $y = 1$.

The effects of model parameters on the Sherwood number Sh at the walls $y = 0$ and $y = 1$ are graphically plotted in Figs. 20–23. Figure 20 presents the simultaneous influence of the pressure gradient A and the chemical reaction parameter $\mathrm{rx} > 0$ on the Sherwood number Sh in the presence of suction and injection at both walls $y = 0$ and $y = 1$ of the microchannel. It is found that the rise of the chemical reaction parameter $\mathrm{rx} > 0$ increases the Sherwood number Sh at both walls of the microchannel with the presence of suction and injection. However, the Sherwood number Sh reduces with an increase in the pressure gradient parameter A at the left wall $y = 0$ and is not appreciably influenced by an increase in the pressure gradient parameter A at the right wall $y = 1$. Figure 21 shows us that a decreasing Sherwood number Sh at the walls $y = 0$ and $y = 1$ as the Eckert number Ec and A_1 augment concurrently. Moreover,

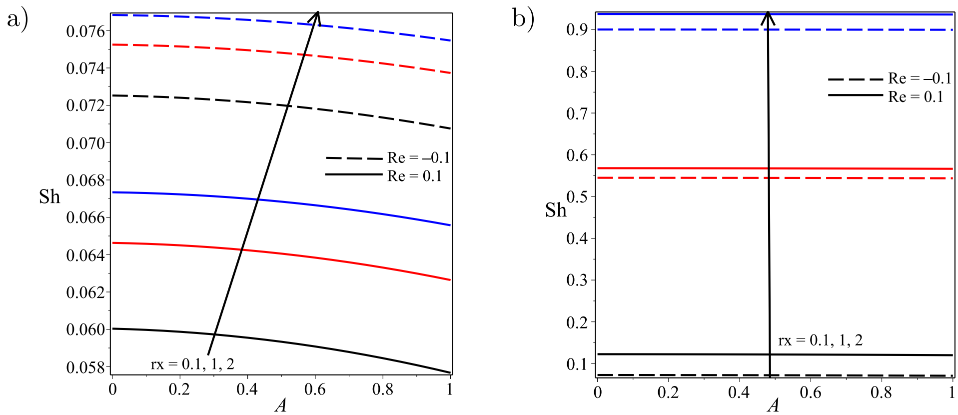

FIG. 20. Sherwood number Sh vs. pressure gradient A with increasing rx and Re: a) at $y = 0$, b) at $y = 1$.

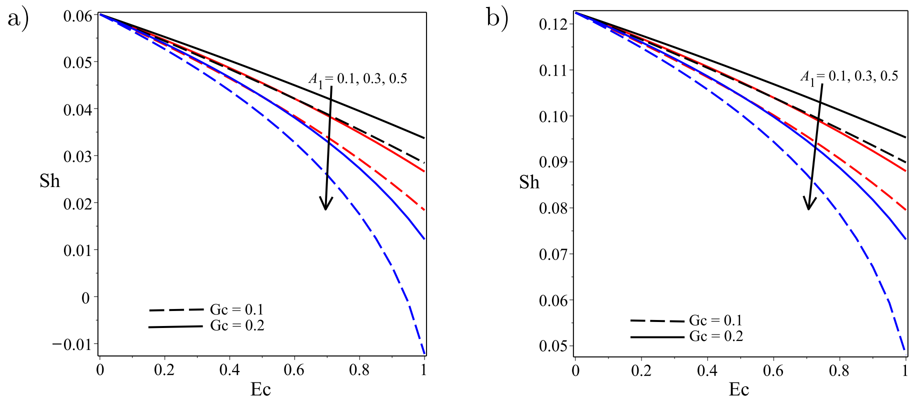

FIG. 21. Sherwood number Sh vs. Eckert number Ec with increasing A_1 and Gc: a) at $y = 0$, b) at $y = 1$.

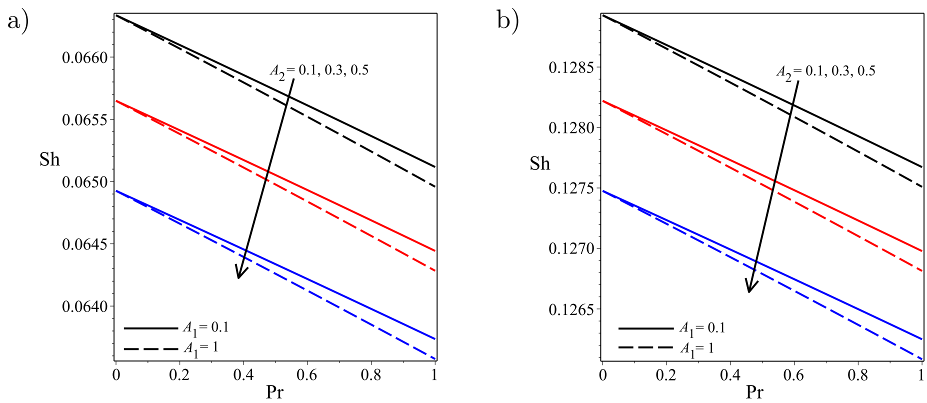

FIG. 22. Sherwood number Sh vs. Prandtl number Pr with increasing A_2 and A: a) at $y = 0$, b) at $y = 1$.

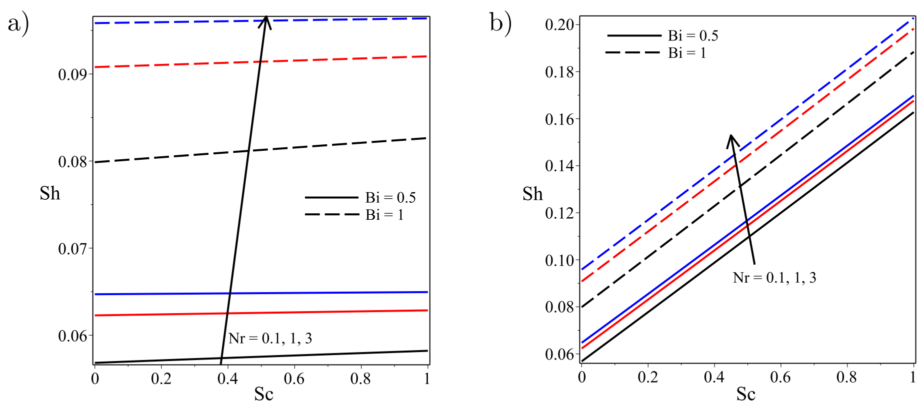

FIG. 23. Sherwood number Sh vs. Schmidt number Sc with increasing Nr and Bi: a) at $y = 0$, b) at $y = 1$.

an increased Sherwood number Sh is observed with an increase in the Grashof number Gc at both walls $y = 0$ and $y = 1$.

The combined effects of the Prandtl number Pr, the thermal conduction variation parameter A_2, and the viscosity variation parameter A_1 on the Sherwood number Sh at the walls $y = 0$ and $y = 1$ are depicted in Fig. 22. It is found that the combined increase of Pr, A_2, and A_1 diminishes the Sherwood number Sh at both walls $y = 0$ and $y = 1$ of the microchannel. The Sherwood number Sh augments at both walls of $y = 0$ and $y = 1$ of the microchannel with the rise of the thermal radiation parameter Nr, the Schmidt number Sc, and the Biot number Bi, as shown in Fig. 23.

5. Summary and conclusions

Unsteady hydromagnetic flow, heat and mass transfer of a water-based nanofluid with variable properties through a permeable microchannel in the presence of the magnetic field, chemical reaction, and thermal radiation were discussed thoroughly. Using appropriate dimensionless variables and parameters, the governing nonlinear PDEs were transformed into a system of non-dimensionalized PDEs and then solved using the semi-discretization method along with the central finite difference and the Runge-Kutta-Fehlberg integration technique. Graphical results are presented and analyzed for various parameter values. The main findings are summarized below.

- The velocity and concentration profiles attained their steady-state velocity and concentration faster than the temperature profiles.
- A dynamic fluctuation of nanoparticle concentration in the fluid near the right wall $y = 1$ of the microchannel was obtained for time t between $0 < t < 2$.
- The nanofluid through the microchannel moved swiftly with an increase in A, A_1, Gc, Gr, Ec, and moved slowly with M, $\mathrm{rx} > 0$ increment.
- The temperature of the nanofluid within the microchannel fell with rise in Nb, Nr, and $\mathrm{Re} < 0$ where as it increases with rise in A_2, Nt, Sc, Ec, and $\mathrm{Re} > 0$.
- The nanoparticle concentration augmented across the microchannel with increasing Ec and $\mathrm{rx} < 0$ and reduced with increasing Sc, Nb, Bi, Nr, and $\mathrm{rx} > 0$.
- Increasing Pr, Bi, Gr, and Gc decreased the skin friction Cf at the left wall $y = 0$ and enhanced Cf at $y = 1$. Moreover, increasing Sc, Nr, M, and $\mathrm{rx} > 0$ enhanced Cf at $y = 0$ and dwindled Cf at $y = 1$.
- The Nusselt number Nu enhanced at both walls $y = 0$ and $y = 1$ of the microchannel with increasing A_2, Bi, Sc, and $\mathrm{rx} > 0$.

- The Sherwood number Sh diminished at both walls $y = 0$ and $y = 1$ of the microchannel with increasing A_1, Ec, A_2, and Pr, but it enhanced at both walls $y = 0$ and $y = 1$ with increasing Bi, Gc, Nr, and $\mathrm{rx} > 0$.

References

1. Abu-Nada E., Oztop H.F., Numerical analysis of Al_2O_3/water nanofluids natural convection in a wavy walled cavity, *Numerical Heat Transfer, Part A: Application Engineering*, **59**(5): 403–419, 2011, doi: 10.1080/10407782.2011.552363.

2. Belhadj A., Numerical investigation of forced convection of nanofluid in microchannels heat sinks, *Journal of Thermal Engineering*, **4**(5): 2263–2273, 2018, doi: 10.18186/thermal.438480.

3. Bellos E., Tzivanidis C., A review of concentrating solar thermal collectors with and without nanofluids, *Journal of Thermal Analysis and Calorimetry*, **135**(1): 763–786, 2011, doi: 10.1007/s10973-018-7183-1.

4. Bowers J., Cao H., Qiao G., Li Q., Zhang G., Mura E., Ding Y., Flow and heat transfer behaviour of nanofluids in microchannels, *Progress in Natural Science: Materials International*, **28**(2): 225–234, 2018, doi: 10.1016/j.pnsc.2018.03.005.

5. Choi S.U., Nanofluid technology: current status and future research, Conference: Korea-U.S. Technical Conference on Strategic Technologies, Vienna, VA, United States, 22–24 Oct. 1998, https://www.osti.gov/servlets/purl/11048.

6. Choi S.U.S., Eastman J.A., Enhancing thermal conductivity of fluids with nanoparticles, *Proceedings of The 1995 ASME International Mechanical Engineering Congress and Exposition*, 1995.

7. Das S.K., Choi S.U.S, Patel H.E., Heat transfer in nanofluids – a review, *Heat Transfer Engineering*, **27**(10): 3–19, 2006, doi: 10.1080/01457630600904593.

8. Gavara M., Asymmetric forced convection of nanofluids in a channel with symmetrically mounted rib heaters on opposite walls, *Numerical Heat Transfer, Part A: Applications*, **62**(11): 884–904, 2012, doi: 10.1080/10407782.2012.707057.

9. Herwig H., Mahulikar S.P., Variable property effects in single-phase incompressible flows through microchannels, *International Journal of Thermal Science*, **45**(10): 977–981, 2006, doi: 10.1016/j.ijthermalsci.2006.01.002.

10. Hindebu B., Makinde O.D., Guta L., Unsteady mixed convection flow of variable viscosity nanofluid in a micro-channel filled with a porous medium, *Indian Journal of Physics*, **96**(6): 1749–1766, 2022, doi: 10.1007/s12648-021-02116-y.

11. Kakaç S., Pramuanjaroenkij A., Review of convective heat transfer enhancement with nanofluids, *Journal of Heat and Mass Transfer*, **52**(13–14): 3187–3196, 2009, doi: 10.1016/j.ijheatmasstransfer.2009.02.006.

12. Karimipour A., Afrand M., Magnetic field effects on the slip velocity and temperature jump of nanofluid forced convection in a microchannel, *Proceedings of the Institution of Mechanical Engineers, Part C Journal of Mechanical Engineering Science*, **230**(11): 1921–1936, 2016, doi: 10.1177/0954406215586232.

13. Kefene M.Z., Makinde O.D., Enyadene L.G., MHD variable viscosity mixed convection of nanofluid in a microchannel with permeable walls, *Indian Journal of Pure & Applied Physics*, **58**(12): 892–908, 2020, doi: 10.56042/ijpap.v58i12.36784.

14. Khan M.G., Fartaj A., A review on microchannel heat exchangers and potential applications, *International Journal of Energy Research*, **35**(7): 553–582, 2011, doi: 10.1002/er.1720.

15. Khodabandeh E., Akbari O.A., Toghraie D., Pour M.S., Jönsson P.G., Ersson M., Numerical investigation of thermal performance augmentation of nanofluid flow in microchannel heat sinks by using of novel nozzle structure: sinusoidal cavities and rectangular ribs, *Journal of the Brazilian Society of Mechanical Sciences and Engineering*, **41**: 443, 2019, doi: 10.1007/s40430-019-1952-z.

16. Kleinstreuer C., Li J., Koo J., Microfluidics of nano-drug delivery, *International Journal of Heat and Mass Transfer*, **51**(23–24): 5590–5597, 2008, doi: 10.1016/j.ijheatmasstransfer.2008.04.043.

17. Kumar A., Nath S., Bhanja D., Effect of nanofluid on thermo hydraulic performance of double layer tapered microchannel heat sink used for electronic chip cooling, *Numerical Heat Transfer, Part A: Applications*, **73**(7): 429–445, 2018, doi: 10.1080/10407782.2018.1448611.

18. Kumar R., Physical effects of variable fluid properties on gaseous slip-flow through a microchannel heat sink, *Journal of Thermal Engineering*, **7**(3): 635–649, 2021, doi: 10.18186/thermal.888496.

19. Lee J., Mudawar I., Assessment of the effectiveness of nanofluids for single-phase and two-phase heat transfer in micro-channels, *International Journal of Heat and Mass Transfer*, **50**(3–4): 452–463, 2007, doi: 10.1016/j.ijheatmasstransfer.2006.08.001.

20. Li J., Kleinstreuer C., Thermal performance of nanofluid flow in microchannels, *International Journal of Heat and Fluid Flow*, **29**(4): 1221–1232, 2008, doi: 10.1016/j.ijheatfluidflow.2008.01.005.

21. Mahulikar S.P., Herwig H., Theoretical investigation of scaling effects from macro-to-microscale convection due to variations in incompressible fluid properties, *Applied Physics Letters*, **86**(014105): 1–3, 2005, doi: 10.1063/1.1845597.

22. Makinde O.D., Heat transfer in variable viscosity micro-channel flow of EG-water/Ag nanofluids with convective cooling, *Defect and Diffusion Forum*, **387**: 182–193, 2018, doi: 10.4028/www.scientific.net/DDF.387.182.

23. Makinde O.D., Eegunjobi A.S., Effects of convective heating on entropy generation rate in a channel with permeable walls, *Entropy*, **15**(1): 220–233, 2013, doi: 10.3390/e15010220.

24. Makinde O.D., Franks O., On MHD unsteady reactive Couette flow with heat transfer and variable properties, *Central European Journal of Engineering*, **4**(1): 54–63, 2014, doi: 10.2478/s13531-013-0139-0.

25. Makinde O.D., Kumar K.G., Manjunatha S., Gireesha B.J., Effect of nonlinear thermal radiation on MHD boundary layer flow and melting heat transfer of micro-polar fluid over a stretching surface with fluid particles suspension, *Defect and Diffusion Forum*, **378**: 125–136, 2017, doi: 10.4028/www.scientific.net/DDF.378.125.

26. Makinde O.D., Ogulu A., The effect of thermal radiation on the heat and mass transfer flow of a variable viscosity fluid past a vertical porous plate permeated by a transverse

magnetic field, *Chemical Engineering Communications*, **195**(12): 1575–584, 2008, doi: 10.1080/00986440802115549.

27. Malvandi A., Ganji D.D., Mixed convection of alumina/water nanofluid in microchannels using modified Buongiorno's model in presence of heat source/sink, *Journal of Applied Fluid Mechanics*, **9**(5): 2277–2289, 2016, doi: 10.18869/acadpub.jafm.68.236.25641.

28. Mohammed H.A., Bhaskaran G., Shuaib N.H., Saidur R., Heat transfer and fluid flow characteristics in microchannels heat exchanger using nanofluids: a review, *Renewable and Sustainable Energy Reviews*, **15**(3): 1502–1512, 2011, doi: 10.1016/j.rser.2010.11.031.

29. Monaledi R.L., Makinde O.D., Entropy analysis of a radiating variable viscosity EG/Ag nanofluid flow in microchannels with buoyancy force and convective cooling, *Defect and Diffusion Forum*, **378**: 273–285, 2018, doi: 10.4028/www.scientific.net/DDF.387.273.

30. Mostafazadeh A., Toghraie D., Mashayekhi R., Akbari O.A., Effect of radiation on laminar natural convection of nanofluid in a vertical channel with single-and two-phase approaches, *Journal of Thermal Analysis and Calorimetry*, **138**(1): 779–794, 2019, doi: 10.1007/s10973-019-08236-2.

31. Na N.Y., *Computational Methods in Engineering Boundary Value Problems*, Academic Press, New York, 1979.

32. Nguyen Q., Bahrami D., Kalbasi R., Bach Q.-V., Nanofluid flow through microchannel with a triangular corrugated wall: heat transfer enhancement against entropy generation intensification, *Mathematical Methods in the Applied Sciences*, 1–14, 2020, doi: 10.1002/mma.6705.

33. Nguyen Q., Sedeh S.N., Toghraie D., Kalbasi R., Karimipour A., Numerical simulation of the ferro-nanofluid flow in a porous ribbed microchannel heat sink: investigation of the first and second laws of thermodynamics with single-phase and two-phase approaches, *Journal of the Brazilian Society of Mechanical Sciences and Engineering*, **42**(492): 1–14, 2020, doi: 10.1007/s40430-020-02534-9.

34. Pati S., Kumar V., Effects of temperature-dependent thermophysical properties on hydrodynamic swirl decay in microtubes, *Proceedings of the Institution of Mechanical Engineers, Part E: Journal of Process Mechanical Engineering*, **233**(3): 427-435, 2019, doi: 10.1177/0954408918755782.

35. Pordanjani A.H., Jahanbakhshi A., Nadooshan A.A., Afrand M., Effect of two isothermal obstacles on the natural convection of nanofluid in the presence of magnetic field inside an enclosure with sinusoidal wall temperature distribution, *International Journal of Heat and Mass Transfer*, **121**: 565–578, 2018, doi: 10.1016/j.ijheatmasstrans fer.2018.01.019.

36. Prasad K.V., Vaidya H., Vajravelu K., MHD mixed convection heat transfer in a vertical channel with temperature-dependent transport properties, *Journal of Applied Fluid Mechanics*, **8**(4): 693–701, 2015, doi: 10.18869/acadpub.jafm.67.223.21562.

37. Rashidi S., Mahaian O., Languri E.M., Applications of nanofluids in condensing and evaporating systems, *Journal of Thermal Analysis and Calorimetry*, **131**(3): 2027–2039, 2018, doi: 10.1007/s10973-017-6773-7.

38. Rikitu B.H., Makinde O.D., Enyadene L.G., Unsteady mixed convection of a radiating and reacting nanofluid with variable properties in a porous medium microchannel, *Archive of Applied Mechanics*, **92**(1): 92–119, 2022, doi: 10.1007/s00419-021-02043-8.

39. Rosseland S., *Astrophysik aud Atom-Theoretische Grundlagen*, Springer, Berlin, 1931, doi: 10.1007/978-3-662-26679-3.

40. Sheikholeslami M., CuO-water nanofluid free convection in a porous cavity considering Darcy law, *The European Physical Journal Plus*, **132**(55): 1–11, 2017, doi: 10.1140/epjp/i2017-11330-3.

41. Sindhu S., Gireesha B.J., Heat and mass transfer analysis of chemically reactive tangent hyperbolic fluid in a microchannel, *Heat Transfer*, **50**(2): 1410–1427, 2021, doi: 10.1002/htj.21936.

42. Snoussi L., Ouerfelli N., Sharma K.V., Vrinceanu N., Chamkha A.J., Guizani A., Numerical simulation of nanofluids for improved cooling efficiency in a 3D copper microchannel heat sink (MCHS), *Physics and Chemistry of Liquids: An International Journal*, **56**(3): 311–331, 2018, doi: 10.1080/00319104.2017.1336237.

43. Sparrow M., Cess R.D., *Radiation Heat Transfer*, Augmented Edition, Routledge, Boca Raton, USA, 1978, doi: 10.1201/9780203741382.

44. Tuckerman D.B., Pease R.F., High performance heat sinking for VLSI, *IEEE Electron Device Letter*, **2**(5): 126–129, 1981, doi: 10.1109/EDL.1981.25367.

45. Ullah I., Shafie S., Makinde O.D., Khan I., Unsteady MHD Falkner-Skan flow of Casson nanofluid with generative/destructive chemical reaction, *Chemical Engineering Science*, **172**: 694–706, 2017, doi: 10.1016/j.ces.2017.07.011.

46. Wang X.-Q., Mujumdar A.S., Heat transfer characteristics of nanofluids: a review, *International Journal of Thermal Science*, **46**(1): 1–19, 2007, doi: 10.1016/j.ijthermalsci.2006.06.010.

47. Yu W., France D.M., Routbort J.L., Choi S.S.U., Review and comparison of nanofluid thermal conductivity and heat transfer enhancements, *Heat Transfer Engineering*, **29**(5): 432–460, 2008, doi: 10.1080/01457630701850851.

Received June 10, 2022; accepted version December 15, 2022.